The bricks of Hagia Sophia (Istanbul, Turkey): a new hypothesis to explain their compositional differences

Mirco Taranto[a], Luis Barba[b], Jorge Blancas[b], Andrea Bloise[a], Marco Cappa[c], Francesco Chiaravalloti[d], Gino Mirocle Crisci[a], Murat Cura[a], Daniela De Angelis[c], Raffaella De Luca[a], Marco Lezzerini[f], Alessandra Pecci[a, e], Domenico Miriello[a, *]

[a] University of Calabria, Department of Biology, Ecology and Earth Sciences, Via P. Bucci, Cubo 12B, 87036 Arcavacata di Rende (CS), Italy.

[b] National Autonomous University of Mexico, Institute of Anthropological Research (IIA), D.F. 04510, Mexico.

[c] Restructura, Surveys for cultural heritage, Via Gerolamo De Rada 60/I, 87100 Cosenza (CS), Italy.

[d] CNR-IRPI Istituto di Ricerca per la Protezione Idrogeologica, Rende (CS), Italy.

[e] University of Barcelona, ERAAUB, Department of History and Archaeology, Spain.

[f] University of Pisa, Department of Earth Sciences, Via S. Maria 53, 56126 Pisa, Italy.

*corresponding author, email: miriello@unical.it.

Highlights

• Bricks from Hagia Sophia (Istanbul, Turkey) were analyzed by OM, XRF, XRPD, TGA, SEM-EDS.

• An innovative micro-EDS approach on the matrix of the bricks showed that different clays were used in different building phases.

• The compositional analogy between the bricks from Hagia Sophia (Istanbul, Turkey) of the 6th and 14th centuries it has been highlighted.

Abstract

The work shows the results of a multi-analytical study performed on twenty-nine brick samples, taken from Hagia Sophia in Istanbul (Turkey). Hagia Sophia, one of the most important historical buildings in the world, has a very complex construction history; this complexity is also reflected in the materials used for its construction. The main purpose of this work is to verify if there are compositional differences in the bricks used in different historical periods, but also to understand the reasons for the eventual compositional differences between one period and another. The samples were studied by optical microscopy (OM), X-ray fluorescence (XRF), X-ray powder diffraction (XRPD) and thermo-gravimetric analysis (TGA), coupled with a new approach, based on the micro-chemical EDS analysis, used to obtain information on the clay fraction of the matrix. The study showed that, most probably, the differences between the bricks belonging to the different construction phases are due to the composition of the clays used for their preparation.

Keywords

Clay; construction phases; discriminant analysis; matrix; compositional characterization

1. **Introduction and research aims**

Hagia Sophia, built in the 4th century AD, is one of the most important buildings in the world. Its constructive history is complex and widely discussed in the scientific literature (Emerson and Van Nice 1950; Underwood & Hawkins 1961; Van Nice 1965; Kinross 1974; Necipoglu 1992; Mainstone 2009; Erdik & Croci 2010; Cappa et al. 2016; Barba et al. 2018). It is possible to summarize its history in 4 major construction phases (Mainstone 2009). The first period dates back to the 4th and 5th century AD; the second period refers to the 5th and 6th century AD; the third phase covers a long time from the 6th to the 14th century AD and the last phase refers to the 15th and 19th centuries AD (Mainstone 2009). However, recent studies on ancient mortars, have shown that it is possible to recognize probable restorations already realized in antiquity, suggesting the presence of more phases (Miriello et al. 2017). In the following centuries, Hagia Sophia was subjected to numerous restoration, reconstruction and consolidation works, many of which are still in progress. Archaeometric studies on natural and artificial stone materials can provide important information on the production technology of the past, on the state of conservation of the materials, on the construction evolution of ancient buildings and also on the commercial relations existing between distant populations (Barca et al. 2013; Miriello et al. 2013; Antonelli et al. 2014; Tema et al. 2015; Bloise et al. 2016; Miriello et al. 2018; Pecci et al. 2018). Hagia Sophia is one of the most studied ancient buildings in the world; many studies have been conducted on his building materials using techniques with different degrees of invasiveness (Cappa et al. 2016; Miriello et al. 2017; Barba et al. 2018; Çakmak et al 1995; Cura et al. 2014; Moropoulou et al. 2000a, 2000b, 2002a, 2002b, 2003, 2006, 2010, 2012a, 2012b, 2013). However, the studies concerning the bricks used in the building are still few and they involved some samples taken from entrance, basement and dome of Hagia Sophia (Moropoulou et al. 2002b). The aim of this study is to improve the knowledge on the bricks of Hagia Sophia through the compositional characterization of samples taken from different places than those studied in the previous works (Moropoulou et al. 2002b). To achieve these goals, in addition to the classic characterization performed by optical microscopy (OM), X-ray fluorescence (XRF), X-ray powder diffraction (XRPD) and thermogravimetric analysis (TGA), a new approach, based on the micro-chemical EDS analysis, was used.

2. Sampling, materials and methods

Twenty-nine brick samples were sampled from different parts of Hagia Sophia. The location of the samples is shown on the 3D model laser scanner (Fig. 1) built by Cura (2016). The probable dating of the samples based on historical studies (Mainstone 2009) is shown in Table 1.

The samples were studied using a multi-analytical approach. The petrographic analysis on thin section was performed by polarized light microscopy with a “Zeiss-Axioskop 40” microscope coupled with a “Canon PowerShot A640” camera.

A point-counter “Meiji Techno MA945”, placed on the table of the polarized microscope, was used for modal analysis to evaluate the percentage (% volume) of matrix, monocrystalline and polycrystalline fragments, porosity (d<1/16 mm), chamotte and secondary calcite inside the pores. For this purpose, a step xy of 1 mm was used on 500 points for thin section.

Thermogravimetric analysis (TGA) was carried out on a Netzsch STA 449 C Jupiter; materials were heated at a rate of 10°C min^{-1} in an alumina crucible under a constant nitrogen flow of 30 cm^3 min^{-1} (Bloise et al. 2009), heating from ambient temperature to 920 °C. Approximately 20 mg of sample was used for each run.

Major (SiO_2, TiO_2, Al_2O_3, Fe_2O_3, MnO, MgO, CaO, Na_2O, K_2O, P_2O_5) and trace (Ni, Cr, V, La, Ce, Co, Ba, Nb, Y, Sr, Zr, Rb) chemical components were determined by X-Ray fluorescence (XRF) on fused glass disks utilizing an ARL 9400 XP+ sequential X-ray spectrometer under the instrumental conditions reported in Lezzerini et al., 2013. Within the range of the measured concentrations, the analytical uncertainties are < 3% for all the components, except for Na_2O, P_2O_5, CaO, TiO_2 and MnO, which may occasionally attain <10 % for very low concentrations (Lezzerini et al., 2013; 2014). XRF analysis was performed on all samples, except for the bricks BAS23, BAS25, BAS28 and BAS29, because the amount of available material was very small. However, for these samples, all the other types of analyses have been performed.

The qualitative mineralogical composition of the samples was studied using a Bruker D8 Advance X-ray powder diffractometer (XRPD) with Cu–Ka radiation, operating at 40 kV and 40 mA. Powder diffraction data were collected in the range 3–60° 2Θ in steps of 0.02° 2Θ (step time 0.4 s). The EVA software program (DIFFRACplus EVA) was used to identify the mineral phases in each X-ray powder spectrum, by comparing experimental peaks with PDF2 reference patterns.

Microchemical analysis of the matrix and volcanic fragments was carried out using an Electron Probe Micro Analyzer JEOL- JXA 8230 coupled with a Spectrometer EDS – JEOL EX-94310FaL1Q; in particular, the micro EDS analyses were performed for each thin section on three representative areas of the matrix 600X600 μm in size.

The software “IBM SPSS statistics release 24” was used to perform multivariate statistical analysis (discriminant analysis).

3. Results and discussion

3.1 Mineralogical and petrographic features

Most of the walls of Hagia Sophia were built using bricks. From the macroscopic point of view, the samples have a rather variable appearance. The color varies from an intense red of the BAS3 sample (Fig. 2a), a soft yellow of the BAS7 (Fig. 2b); although it is also possible to observe the pink color in the sample BAS 28 (Fig. 2c). However, in the first analysis, from the study of macroscopic color, we can only say that the samples were fired in an oxidizing atmosphere. In fact, color is not a variable that allows to make compositional considerations, since the same fabric cooked in the same kiln can derive bricks of different color depending on the different spatial distribution inside it (Miriello et al. 2007).

The observation of all samples with the naked eyes shows the presence of millimeter sized vacuoles and rare clasts of greater than 3 mm in size.

The mineralogical and petrographic observation in thin section shows the presence of a rather homogeneous mineralogy for all the samples (Table 2). Generally, quartz prevails (Fig. 3a) followed, in order of decreasing abundance, from plagioclase (3b), orthoclase (3c), micas as muscovite (Fig. 3d) and biotite (Fig. 3e), and opaque minerals. The calcite found in most of the samples is due to recrystallization phenomena of secondary calcite in the pores (Fig. 3f); only in the sample BAS12 its presence can be attributed to rare fragments of bioclasts (Fig. 3g).. The modal analysis allowed to estimate the content of secondary calcite in the pores, ranging from a minimum of 0.93% for the BAS20 sample to a maximum of 10.18% for the BAS12 sample (Table 3). Optical microscopy with transmitted polarized light has detected the presence of rare primary pyroxenes (traces); while X-ray powder diffraction (XRPD) allowed to detect the presence of pyroxenes (diopside) in most samples (Table 4). This means that the pyroxenes present in the bricks of Hagia Sophia are found in the form of micrometric

crystals (Miriello et al., 2015) formed secondarily after reaching temperatures above 900 °C during the firing phase. XRPD also allowed to detect the presence of hematite in most of the samples, confirming the firing conditions in an oxidizing atmosphere.

In all samples, the presence of quartzites (Fig. 3h) prevails over the granite rocks (Fig. 3I) and phyllites. The volcanic rocks are found in trace content in some samples (Table 2). The composition of the volcanic rocks, studied by EDS microanalysis, varies from trachy-basalts (Fig. 3L) to rhyolites (Fig. 3M). In most of the samples, the presence of chamotte (Fig. 3n) was found, almost always in traces, except for samples BAS4 and BAS25, where respectively represents 11.60% and 5.12% of the skeleton (Table 3). Non-plastic elements have a sphericity variable from low to high (Powers 1953). The sorting is variable from "poorly sorted" to "well sorted" (Boggs, 2010; Jerram, 2001); in general, for all samples the average particle size of the non-plastic elements is that of the sands, which vary from fine to coarse, except for the sample BAS29 in which a Wentwort size (1922) "coarse silt" is found. The matrix/non-plastic elements ratios vary from a minimum of 2.30 (sample BAS19) to a maximum of 28.17 (sample BAS6) (Table 2).

All the bricks studied were taken from walls of which the dating is well known (Mainstone 2009). This dating was also confirmed by recent studies on the mortar of Hagia Sophia (Miriello et al 2017). This means that bricks can be very well assigned to different construction phases (Table 1). For a better understanding of the compositional data, it is possible to assign the same symbol to the samples belonging to the same construction phase and using a discriminant model based on the variables estimated by the modal analysis (Table 3); the result of the discriminant analysis is shown in Figure 4; this figure shows as there is a partial overlap between the samples belonging to the different construction phases. Only the samples belonging to the 10th century separate themselves from the others; this means that there are small compositional differences between the various samples linked to the mineralogical and petrographic features.

3.2 *Geochemical features of the bulk samples*

The chemical composition, performed by XRF analysis, regards all the samples with the exception of the bricks BAS23, BAS25, BAS28 and BAS29, because the amount of available material was very small. The maximum variability of the chemical elements concerns variables whose concentration is greater; in particular, for the chemical major elements, SiO_2, CaO and Al_2O_3 (Table 5). The greater chemical variability of trace elements regards, in decreasing order, Cr, Ni, Sr, Ba, Zr and V (Table 6). The binary diagrams CaO vs SiO_2 (Fig. 5a) and Sr vs Zr (Fig. 5b) show a good separation between the construction phases, except for samples belonging to the 6th century, which overlap with those belonging to the 14th century; this overlap can be explained assuming that the bricks prepared in the 6th century were reused to rebuild the 14th century walls, collapsed due to a seismic event; this hypothesis is reasonably plausible, because the walls of Hagia Sophia of the 14th century are close to the walls of the 6th century and they have been involved in earthquakes (Charanis 1938; Cutler 1968; Mainstone 2009; Cappa et al. 2016; Cura et al 2016; Miriello et al., 2017). For this reason, from here on out, in the next figures the same symbol will be assigned to the samples of the 6th and 14th centuries. The discriminant analysis, performed by considering all the major and trace chemical elements, confirms very good the strong separation of the samples belonging to different historical periods (Fig. 5c and Fig. 5d). The data show that the discrimination between the different construction phases is better observed using chemical data, rather the modal data obtained from optical microscopy; in the first analysis, this could mean that the different geochemical features of the samples are most probably due to the chemical composition of the matrix, which always represents, on average, about 80% by volume of the sample.

3.3 Thermogravimetric analysis and comparison with the bricks of Rhodes

Thermogravimetric analysis (TGA) was performed in the temperature range between 20 and 920 °C; the results are shown in Table 7. The graph in figure 6a shows the result of the discriminant analysis performed by the data obtained from the thermogravimetric analysis, using all the variables present in Table 7. Figure 6a, confirms the good separation between the different construction phases already highlighted by the previous data.
Regarding the hypothesis of provenance of the clays used to produce the Hagia Sophia bricks, compositional studies on clays in the surroundings of Istanbul are not present in literature; it is possible to use the study by Moropoulou et al. (2002b) to make some very preliminary hypotheses about brick provenance. In this work (Moropoulou et al. 2002b), some samples from the Great Basilica of Rhodes were studied by TGA analysis. Figure 6b shows the SBW (structurally bound water) vs. CO_2 diagram, obtained by TGA data (Table 7); in this diagram the samples of Hagia Sophia were compared with those coming from the Great Basilica of Rhodes (Moropoulou et al. 2002b). The compositional field of Rhodes bricks shows high compositional variability (Fig. 6b), which, in general, differs from that of Hagia Sophia bricks, except for the samples BAS6, BAS17, BAS18, BAS20 and BAS29. However, this apparent analogy is not strong; in fact, the observation of Hagia Sophia bricks in thin sections revealed, for many of them, the presence of secondary calcite in the micro pores (Fig. 3f). The presence of secondary calcite increases the CO_2 content abnormally, translating the Hagia Sophia samples to the compositional field of the Rhodes samples. It can therefore be concluded that for the samples studied in this work no bricks produced with raw materials from Rhodes have been used.

3.4 Microchemical composition of the matrix

The data previously discussed show that the Hagia Sophia bricks are compositionally different in various constructive epochs. This do not seem to be related to strong mineralogical and petrographic differences observable by optical microscopy under transmitted polarized light; if that's true, then, the compositional differences must be preserved even if only the chemical composition of the clay fraction is studied. In fact, the most plausible hypothesis to explain the different compositional features of the bricks is that different types of clays have been used for each construction phase. To deepen this aspect, we have developed a new protocol, which is based on the identification of homogeneous areas of the matrix with a low concentration of non-plastic elements by polarizing optical microscope (Fig. 7a) and their study through micro chemical EDS analysis on area 600x600 μm^2 in size (Fig. 7b). On each sample, three homogeneous areas were identified and subsequently the mean chemical composition of the major elements was calculated (Table 8). Figure 7c shows the results of the discriminant analysis obtained using all the chemical variables present in Table 8. The graph shows a perfect separation of the bricks (Fig. 7c), which matches with the construction phases already identified previously. This reinforces the hypothesis that, even when micro-chemical data representative of the clay composition is used, clays of different compositions have been used in each historical period.

4. Conclusions

This study allows to demonstrate the compositional analogy between the bricks of the walls of the 6th and 14th centuries. The bricks, which were believed to belong to a 14th century wall, were most likely produced in the 6th century and re-used in the 14th c. walls. In fact, it is possible that during the reconstruction of the 14th century, the bricks of the 6th century that were collapsed during a seismic event, were re-used.

The samples, although apparently homogeneous among themselves from the minero-petrographic point of view, have instead revealed significant compositional differences in the finer component, related to the clays used for their production. A new analytical protocol based on micro chemical-EDS analysis of homogeneous areas (free of non-plastic elements), implemented specifically for this work, has allowed to establish that different composition clays have likely been used for each construction period. Moreover, it allowed to group the samples into four compositionally similar sets: samples from the 4th century, samples from the 5th century, samples from the 6th and 14th century, samples from the 10th century.

The results show that the micro chemical study of the matrix can be an excellent tool to formulate hypotheses on the types of clays used in the production of the bricks. This approach should be applied routinely, together with the analysis in thin section performed by optical microscopy under transmitted polarized light, to obtain information useful to solve provenance problems.

The preliminary compositional comparison, based on the thermo-gravimetric analysis (TGA), between the bricks studied in this work and those of the Great Basilica of Rhodes studied by Moropoulou et al. (2002b), allowed to exclude their provenance from Rhodes. It is very likely that local raw materials were used for their production; however, to confirm this hypothesis, mineralogical and geochemical studies of the local clay quarries must be performed.

Acknowledgments

We would like to thank all the staff and the Direction of the Hagia Sophia Museum for their helpfulness and hospitality, as well as the Ministry of Culture of Turkey for the granting of all permits necessary to conduct investigations inside the monument. The work is part of the research activity of the Department of Biology, Ecology and Earth Sciences (DiBEST) of the University of Calabria, the Archaeological Prospection Laboratory, Universidad National Autónoma de México (UNAM), the Ramon y Cajal contract of A. Pecci RYC 2013-13369 and the ERAAUB (Consolidated Group 2014 SGR845) and was carried out within the framework of Mirco Taranto's Ph.D. work. We would also like to thank Mariano Davoli of the Laboratory of Electronic Microscopy and Microanalysis (CM2) of the DiBEST and Giancarlo Niceforo for their support on micro-EDS and XRPD analyses.

REFERENCES

Emerson W., Van Nice R. L. (1950). Hagia Sophia and the First Minaret Erected after the Conquest of Constantinople. American Journal of Archaeology, 54(1), 28-40.

Underwood P. A., Hawkins E. J. (1961). The Mosaics of Hagia Sophia at Istanbul: The Portrait of the Emperor Alexander: A Report on Work Done by the Byzantine Institute in 1959 and 1960. Dumbarton Oaks Papers, 187-217.

Van Nice R. L., Dumbarton Oaks Research Library & Collection (Washington). Center for Byzantine Studies. (1965). Saint Sophia in Istanbul: an architectural survey. Dumbarton Oaks Publ. Service. Washington.

Kinross J. (1974). SANTA SOFIA. Mondadori editore. Milano.

Necipoglu G (1992) The life of an imperial monument: Hagia Sophia after Byzantium. In: Mark R, Cakmak AS (eds) Hagia Sophia from the age of Justinian to the present. Cambridge University Press, Cambridge, pp. 195–225

Mainstone R. J. (2009). Santa Sofia. Electa. Milano.

Erdik M., Croci G. (2010). Earthquake performance of Hagia Sophia: a review of investigations. Annual of Hagia Sophia Museum, 13, 101-134.

Cappa M., De Angelis D., Pecci A., Barba L., Cura M., Crisci G. M., Blancas J., Yavuz H.B., Miriello D. (2016). Thermographic survey at Hagia Sophia: main arches, pendentives and tympana. International Journal of Architectural Heritage, 10(6), 726-734.

Miriello D., Barba L., Blancas J., Bloise A., Cappa M., Cura M., De Angelis D., De Luca R., Pecci A., Taranto M. Yavuz H.B., Crisci G.M. (2017). New compositional data on ancient mortars from Hagia Sophia (Istanbul, Turkey). Archaeological and Anthropological Sciences, 9(4), 499-514.

Barba L., Blancas J., Pecci A., Miriello D., Cura M., Crisci G.M., Cappa M., De Angelis D., Yavuz H. B. (2018). Georadar investigations in the central nave of Hagia Sofia, Istanbul (Turkey). Archaeological and Anthropological Sciences, 10(2), 259-268.

Barca D., Miriello D., Pecci A., Barba L., Ortiz A., Manzanilla L.R., Blancas J., Crisci G.M. 2013. Provenance of glass shards in archaeological lime plasters by LA-ICP-MS: Implications for the ancient routes from the Gulf of Mexico to Teotihuacan in Central Mexico. Journal of Archaeological Science, 40(11), 3999-4008.

Miriello D., Lezzerini M., Chiaravalloti F., Bloise A., Apollaro C., Crisci G.M. 2013. Replicating the chemical composition of the binder for restoration of historic mortars as an optimization problem. Computers and Concrete, 12(4), 553-563.

Antonelli F., Columbu S., Lezzerini M., Miriello D. 2014. Petrographic characterization and provenance determination of the white marbles used in the Roman sculptures of Forum Sempronii (Fossombrone, Marche, Italy). Applied Physics A: Materials Science and Processing, 115(3), 1033-1040.

Tema E., Georgios Polymeris G., Morales J., Goguitchaichvili A., Vassiliki Tsaknaki V. 2015. Dating of ancient kilns: A combined archaeomagnetic and thermoluminescence analysis applied to a brick workshop at Kato Achaia, Greece. Journal of Cultural Heritage, 16(4), 496-507.

Bloise A., Abd El Salam S., De Luca R., Crisci G.M., Miriello D. 2016. Flux growth and characterization of cuprorivaite: the influence of temperature, flux, and silica source. Applied Physics A: Materials Science and Processing, 122(7), Article number 650.

Miriello D., Bloise A., Crisci G.M., De Luca R., De Nigris B., Martellone A., Osanna M., Pace, R., Pecci A., Ruggieri N. 2018. Non-destructive multi-analytical approach to study the pigments of wall painting fragments reused in mortars from the archaeological site of Pompeii (Italy). Minerals, 8(4), Article number 134.

Pecci A., Miriello D., Barca D., Crisci G.M., De Luca R., Ortiz, A., Manzanilla L.R., Blancas J., Barba, L. 2018. Identifying a technological style in the making of lime plasters at Teopancazco (Teotihuacan, México). Archaeological and Anthropological Sciences, 10, 315-335.

Çakmak AŞ., Moropoulou A., Mullen CL. (1995) Interdisciplinary study of dynamic behaviour and earthquake response of Hagia Sophia. Soil Dyn Earthq Eng, 14, 125–133.

Cura M., Pecci A., Miriello D., Barba L., Cappa M., De Angelis D., Blancas J., Crisci G.M. (2014) Multi-analytical approach for the diagnostic at Hagia Sophia: a 3D multimedia database proposal. Annual of Hagia Sophia Museum, 14, 379–403.

Moropoulou A., Bakolas A., Bisbikou K. (2000a) Investigation of the technology of historic mortars. J. Cult. Herit., 1, 45–58.

Moropoulou A., Bakolas A., Moundoulas P., Anagnostopoulou S., Aggelakopoulou E. (2000b). Compatible Restoration Mortars for the Earthquake Protection of Hagia Sophia, PACT, J. European Study Group on Physical, Chemical, Biological and Mathematical Techniques Applied to Archaeology, 59, 29-51.

Moropoulou A., Cakmak AS., Biscontin G., Bakolas A., Zendri E. (2002a) Advanced Byzantine cement based composites resisting earthquake stresses: the crushed brick y lime mortars of Justinian's Hagia Sophia. Constr. Build. Mater., 16, :543–552.

Moropoulou A., Cakmak A., Polikreti K. 2002b. Provenance and Technology Investigation of Agia Sophia Bricks, Istanbul, Turkey. J. Am. Ceram. Soc., 85(2), 366-372.

Moropoulou A., Polikreti K., Bakolas A., Michailidis P. (2003). Correlation of physicochemical and mechanical properties of historical mortars and classification by multivariate statistics. Cement and Concrete Research, 33, 891-898.

Moropoulou A., Labropoulos K., Moundoulas P., Bakolas A. (2006). The contribution of historic mortars on the earthquake resistance of Byzantine monuments. In: Konsta-Gdoutos MS (ed.) Measuring, monitoring and modeling concrete properties. Springer, Netherlands, pp. 643–652.

Moropoulou A., Polikreti K. (2010). Studying the Hagia Sofia structural materials: the conservation of the national technical University of Athens to the monument's protection. Annual of Hagia Sofia Museum, 13, 155–176.

Moropoulou A., Labropoulos K.C., Katsiotis N.S. (2012a). Assessing the Preservation State and Revealing Plastered Mosaics in Hagia Sophia Using Ground Penetrating Radar. Journal of Materials Science and Engineering A., 2, 183-189.

Moropoulou A., Labropoulos K.C., Katsiotis N.S. (2012b). Application of Ground Penetrating Radar for the Assessment of the Decay State of Hagia Sophia's Mosaics. Emerging Technologies in Non-Destructive Testing V, Paipetis et al. (eds.), Taylor e Francis Group, London, 25-30.

Moropoulou A., Bakolas A., Karoglou M., Delegou E.T., Labropoulos K.C., Katsiotis N.S. (2013). Diagnostics and Protection of Hagia Sophia Mosaics. Journal of Cultural Heritage, 14, 133-139.

Cura M. (2016). Costruzione di un database GIS 3D per un approccio multidisciplinare alla diagnostica di Santa Sofia (Istanbul - Turchia). Tesi dottorato Università della Calabria.

Bloise, A., Barrese E., Apollaro C., Miriello D. 2009. Flux growth and characterization of Ti- and Ni-doped forsterite single crystals. Cryst. Res. Technol., 44(5), 463–468.

Lezzerini M., Tamponi M., Bertoli M. (2013). Reproducibility, precision and trueness of X-ray fluorescence data for mineralogical and/or petrographic purposes. Atti Soc. Tosc. Sci. Nat. Mem., Serie A, 120, 67-73.

Lezzerini M., Tamponi M., Bertoli M. (2014). Calibration of XRF data on silicate rocks using chemicals as in house standards. Atti Soc. Tosc. Sci. Nat., Mem., Serie A, 121, 65-70.

Miriello D., Crisci G.M. (2007). The mixing and provenance of raw materials in the bricks from the Svevian castle of Rocca Imperiale (North Calabria - Italy). European Journal of Mineralogy, 19, 137-144.

Miriello D., Bloise A., De Luca R., Apollaro C., Crisci G.M., Medaglia S., Taliano Grasso (2015). First compositional evidences on the local production of Dressel 2–4 amphorae in Calabria (Southern Italy): characterization and mixing simulations. Applied Physics. A, Materials Science & Processing, 119, 1595-1608.

Powers M.C. (1953). A new roundness scale for sedimentary particles J. Sediment. Res., 23, p. 2.

Boggs S. Jr. (2010). Petrology of Sedimentary Rocks (II edition), Cambridge University Press, Cambridge UK.

Jerram D.A. (2001). Visual comparators for degree of grain-size sorting in two and three-dimensions Comput. Geosci., 27, 485-492.

C.K. Wentworth (1922). A scale of grade and class terms for clastic sediments J. Geol., 30, 377-392.

Charanis P. (1938). les βραχεα χρονικα comme source historique. Byzantion, 13(1), 335-362.

Cutler A. (1968). The De Signis of Nicetas Choniates. A Reappraisal. American Journal of Archaeology, 72(2), 113-118.

FIGURES

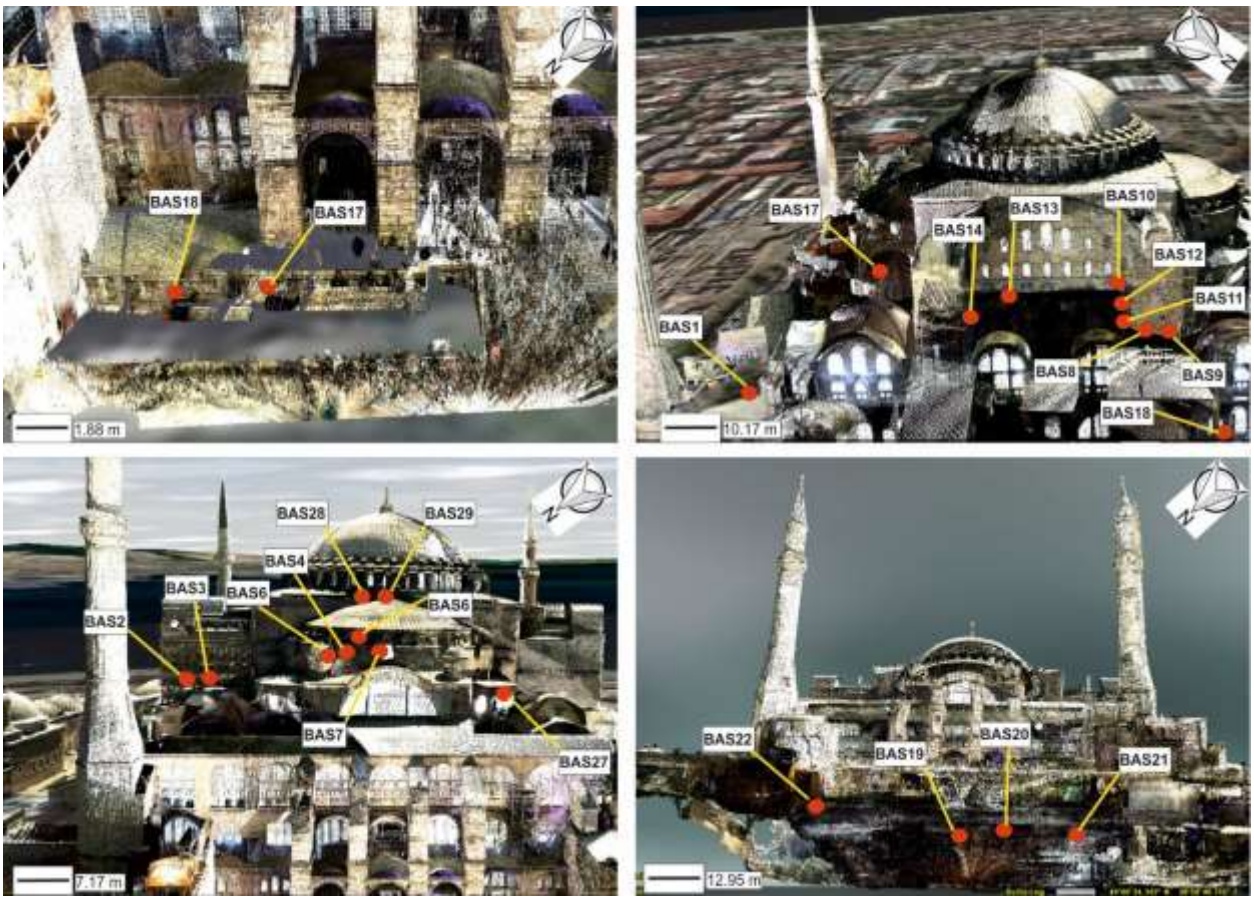

Figure 1 Sampling points of the bricks placed on 3D model laser scanner of Hagia Sophia (Curat 2016).

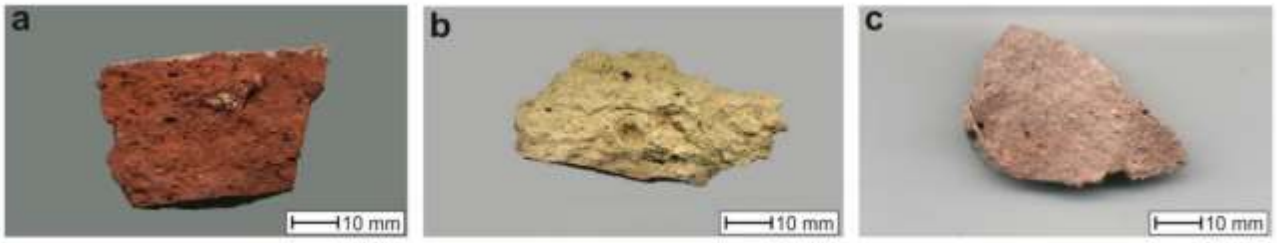

Figure 2 An example of macro photos under reflected light of the bricks of Hagia Sophia representative of the qualitative chromatic features. a) Sample BAS3; b) Sample BAS7; c) Sample BAS28.

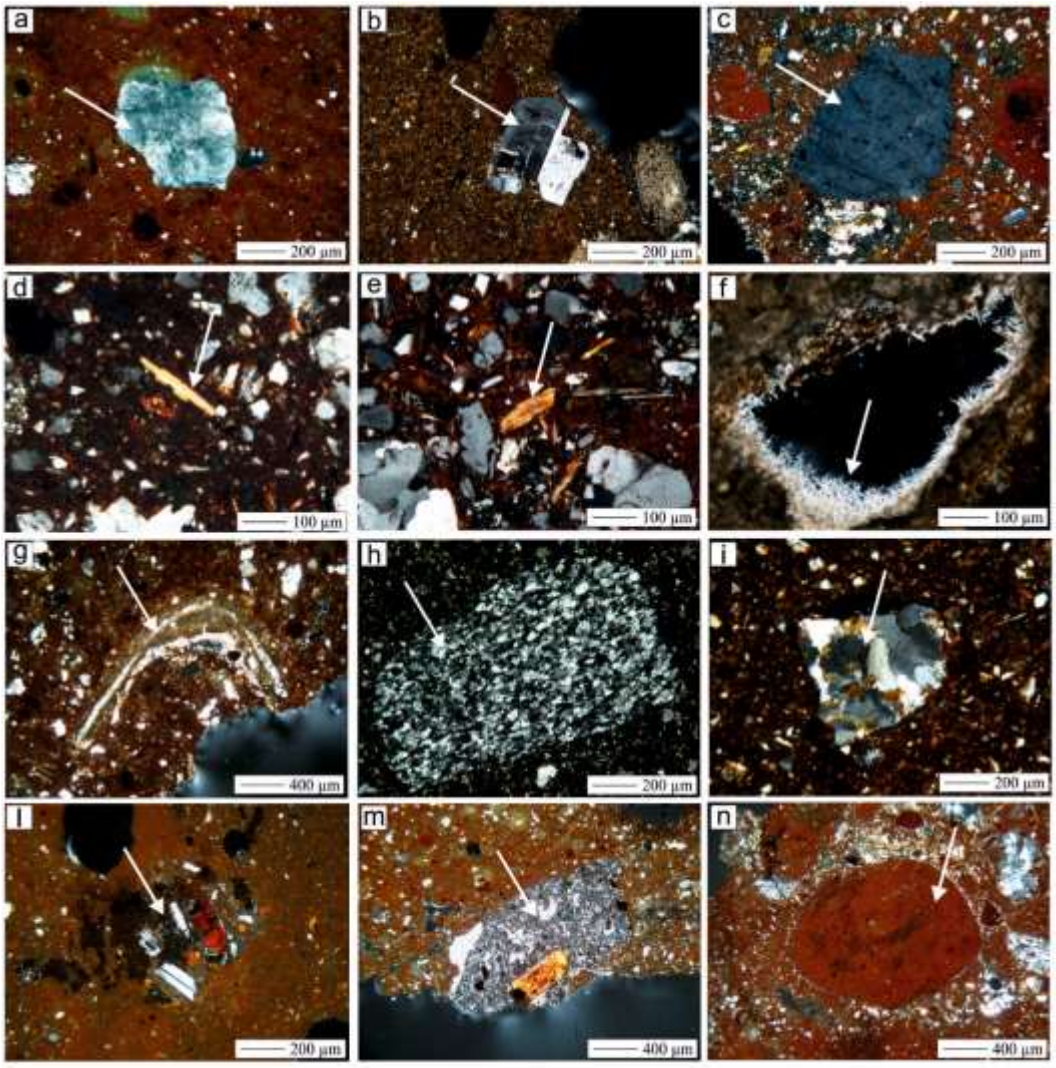

Figure 3 Microphotos performed by optical microscopy under transmitted polarized light of the bricks of Hagia Sophia, crossed nicols. a) Quartz in the sample BAS10; b) Plagioclase in the sample BAS8; c) Orthoclase in the sample BAS9; d) Muscovite in the sample BAS19; e) Biotite in the sample BAS19; f) Secondary calcite in the sample BAS12; g) Bioclast in the sample BAS12; h) Quartzite in the sample BAS7; i) Granite in the sample BAS4; l) Trachy-basalt in the sample BAS22; m) Rhyolite in the sample BAS10; n) Chamotte in the sample BAS16.

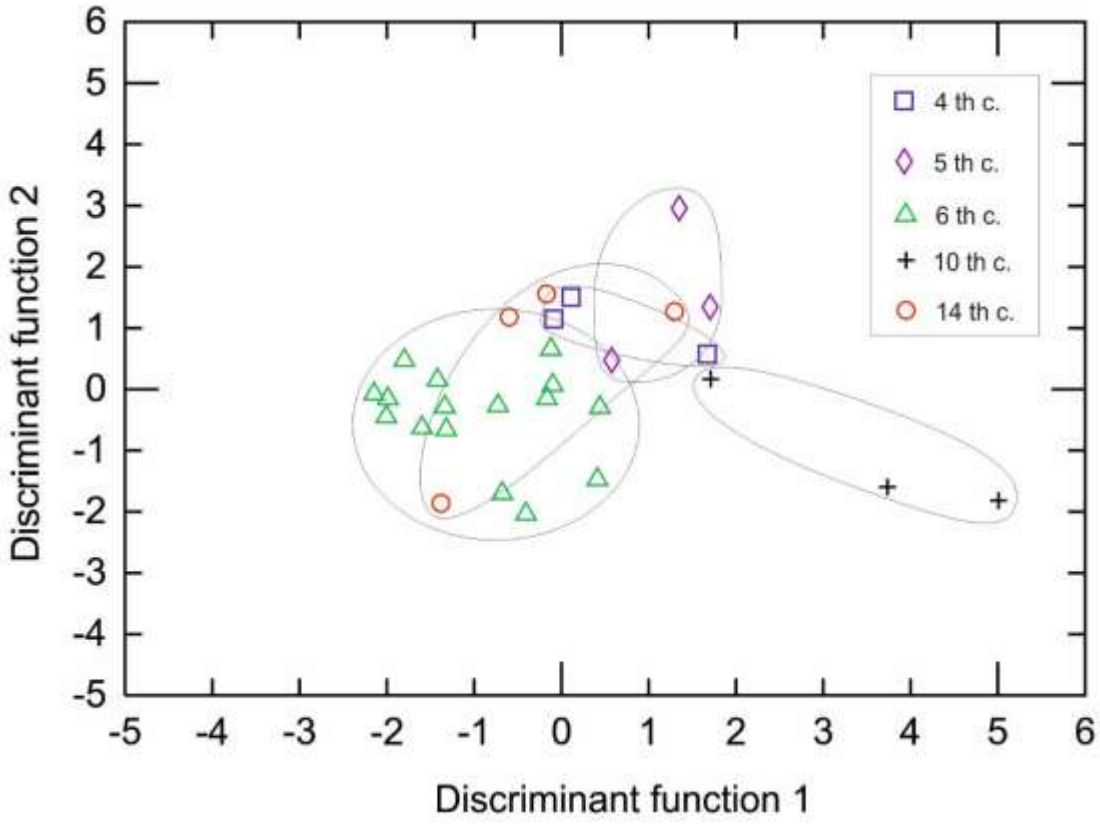

Figure 4 Discriminant analysis of the bricks of Hagia Sophia performed using all modal analysis data (Table 3).

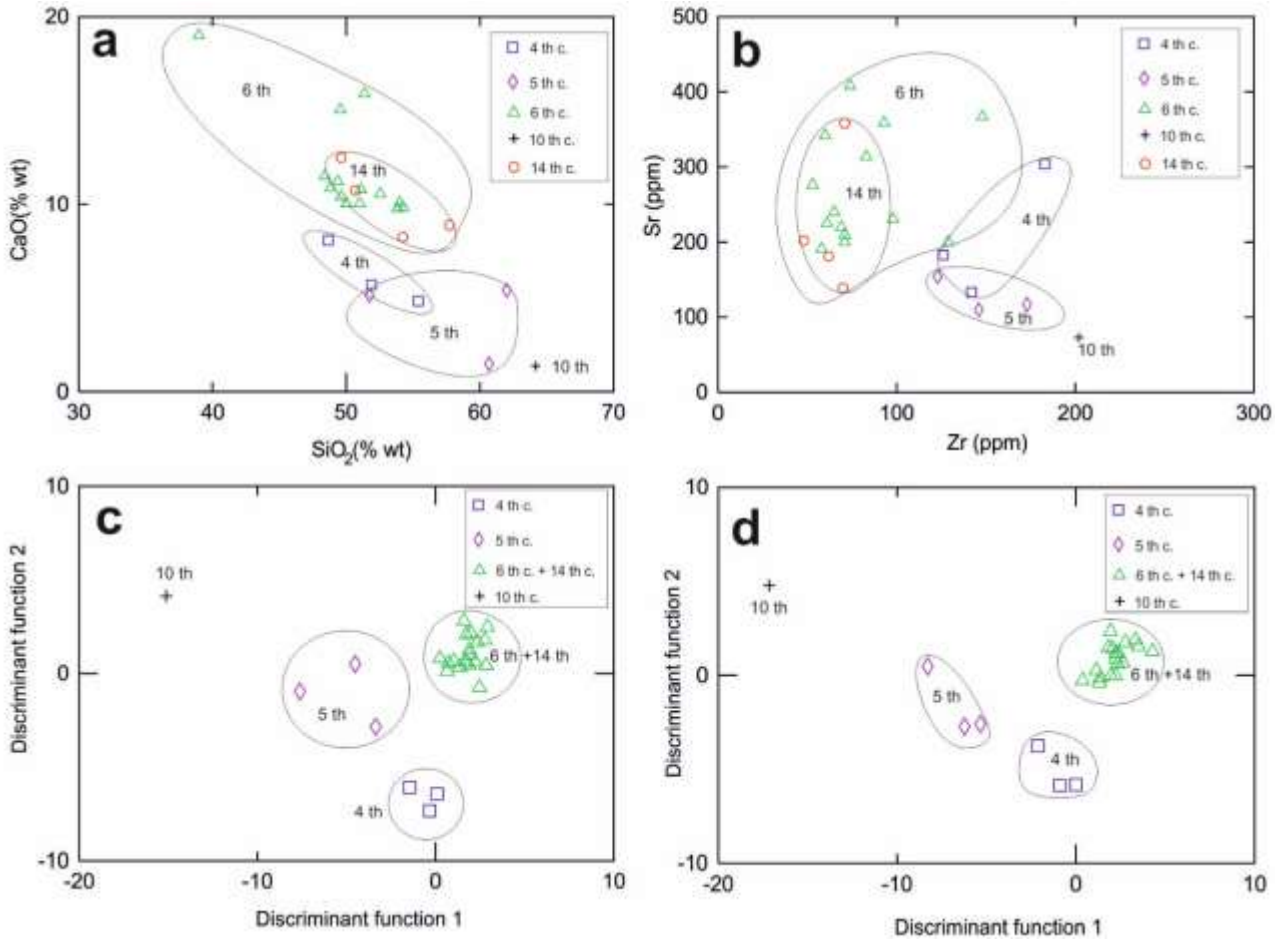

Figure 5 a) Bi-plot diagram CaO vs SiO_2 of the bricks of Hagia Sophia by XRF analysis of the bulk sample; b) Bi-plot diagram Sr vs Zr of the bricks of Hagia Sophia by XRF analysis of the bulk sample; c) Discriminant analysis of the bricks of Hagia Sophia performed using all chemical major elements of the bulk sample, except LOI and P_2O_5; d) Discriminant analysis of the bricks of Hagia Sophia performed using all chemical trace elements of the bulk sample.

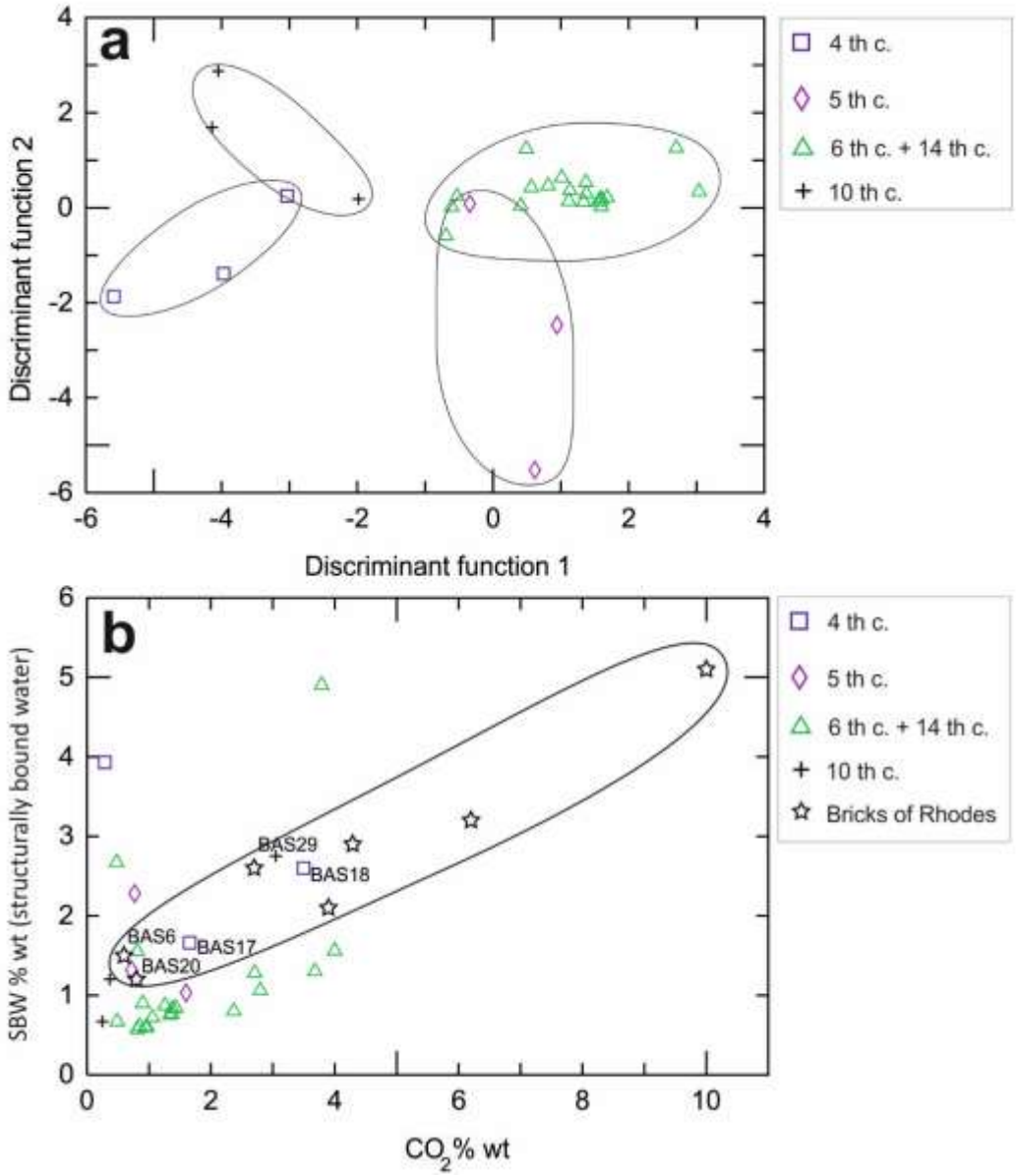

Figure 6 a) Discriminant analysis of the bricks of Hagia Sophia performed using all TGA data (Table 7); b) Bi-plot diagram SBW (structural bound water) vs CO_2 of the bricks of Hagia Sophia obtained by TGA analysis and comparison with the TGA data of the bricks of Great Basilica of Rhodes (Moropoulou et al., 2002b).

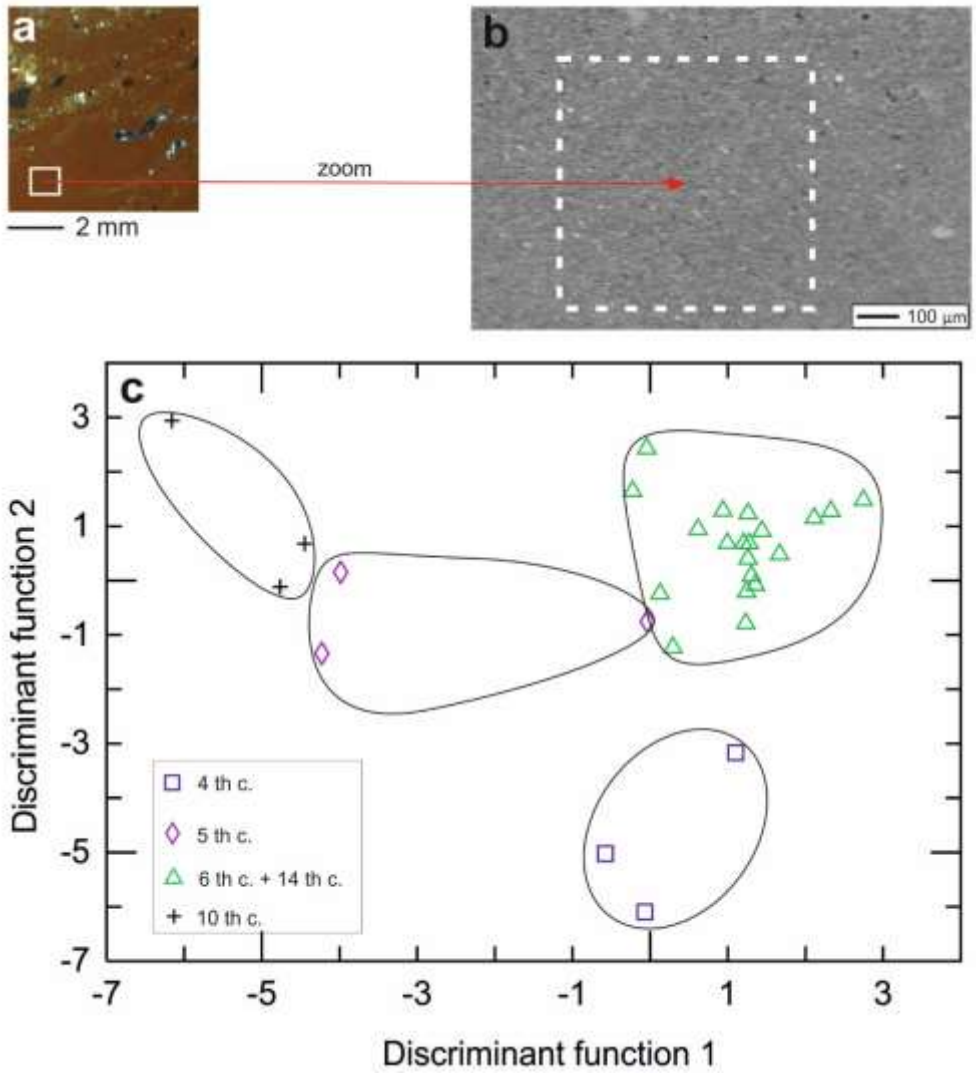

Figure 7 a) Microphotos of the sample BAS24 performed by polarized optical microscopy under crossed nicols; the white square represents a homogeneous area of the matrix with a low concentration of non-plastic elements; b) SEM image of the area of 600x600 micron^2 in size for the sample BAS24 used for micro EDS analysis; c) Discriminant analysis of the bricks of Hagia Sophia, performed using all the chemical major elements obtained by micro chemical EDS analysis (Table 8).

TABLES

	Tipology	Probable dating based on historical studies
BAS1	Brick	6 th c.
BAS2	Brick	6 th c.
BAS3	Brick	10 th c.
BAS4	Brick	6 th c.
BAS5	Brick	6 th c.
BAS6	Brick	6 th c.
BAS7	Brick	6 th c.
BAS8	Brick	6 th c.
BAS9	Brick	6 th c.
BAS10	Brick	6 th c.
BAS11	Brick	14 th c.
BAS12	Brick	6 th c.
BAS13	Brick	6 th c.
BAS14	Brick	6 th c.
BAS15	Brick	6 th c.
BAS16	Brick	6 th c.
BAS17	Brick	4 th c.
BAS18	Brick	4 th c.
BAS19	Brick	5 th c.
BAS20	Brick	5 th c.
BAS21	Brick	5 th c.
BAS22	Brick	4 th c.
BAS23	Brick	6 th c.
BAS24	Brick	14 th c.
BAS25	Brick	6 th c.
BAS26	Brick	14 th c.
BAS27	Brick	14 th c.
BAS28	Brick	10 th c.
BAS29	Brick	10 th c.

Table 1 The bricks taken from Hagia Sophia with probable dating based on historical studies (Mainstone 2009).

				By Modal analysis					By XRPD and EDS						
	Mean non-plastic inclusions size (µm)	Max. non-plastic inclusions size (µm)	Wentworth size (Wentworth 1922)	% Non-plastic inclusions (size>1/16 mm)	% Matrix (size<1/16 mm)	Matrix/non-plastic inclusions ratio	% Porosity (size>1/16 mm mm)	% Secondary calcite	Mineralogical phases of the non-plastic inclusions	Rock fragments	Sorting of non plastic inclusions (by Boggs 2010; Jerram 2001)	Isotropy of the matrix	Roundness (Powers 1953)	Sphericity (Powers 1953)	Chamotte
BAS1	67	693	Very Fine Sand	3.60	88.75	24.66	2.25	5.40	Qtz, Pl, Di, Cal, Hem, Ms, Bt, Om	Quartzites, granites	MWS	Low	Sub-rounded	Low sphericity	P
BAS2	700	2400	Coarse sand	7.29	78.47	10.76	6.08	8.16	Qtz, Pl, Di, Hem, Cal, Bt, Ms, Om	Quartzites, phyllites, basaltic trachy-andesites (traces), trachy-andesites (traces), dacites (traces)	VWS	High	Sub-rounded	Low sphericity	A
BAS3	580	5600	Coarse sand	18.22	75.03	4.12	5.73	1.02	Qtz, Pl, Hem, Or, Ms, Bt, Cal, Om	Quartzites, granites, dacites (traces)	MWS	High	Rounded	Low sphericity	P
BAS4	200	2697	Medium Sand	22.57	66.93	2.97	4.39	6.11	Qtz, Pl, Or, Di, Cal, Ms, Bt, Hem, Om	Quartzites, granites, phyllites	PS	Low	Angular	High sphericity	P
BAS5	440	1220	Medium Sand	5.84	85.06	14.56	3.25	5.84	Qtz, Cal, Di, Pl, Or, Hem, Ms, Bt, Om	Quartzites, granites, phyllites	MWS	High	Angular	High sphericity	A
BAS6	49	1619	Coarse Silt	3.06	86.08	28.17	4.24	6.62	Qtz, Di, Pl, Or, Hem, Bt, Ms, Cal, Om	Quartzites, phyllites	WS	Medium	Angular	High sphericity	A
BAS7	184	6000	Very Fine Sand	12.92	75.42	5.84	4.63	7.02	Qtz, Di, Pl, Cal, Or, Mc, Ms, Bt, Om	Quartzites, phyllites, granites	PS	Very Low	Sub-angular	High sphericity	P
BAS8	238	1303	Fine Sand	7.32	84.36	11.52	4.66	3.66	Qtz, Pl, Or, Di, Cal, Ms, Bt, Hem, Om	Quartzites, basaltic trachy-andesites (traces)	PS	Medium	Sub-angular	High sphericity	P
BAS9	214	2240	Fine Sand	11.17	71.99	6.45	7.39	9.45	Qtz, Pl, Di, Or, Cal, Hem, Ms, Bt, Om	Quartzites, granites, rhyolites (traces)	MWS	Medium	Sub-angular	High sphericity	A
BAS10	630	2370	Coarse Sand	8.56	83.66	9.77	4.28	3.50	Qtz, Di, Pl, Ms, Hem, Cal, Om	Quartzites, phyllites, rhyolites (traces)	MS	Medium	Sub-rounded	Low sphericity	A
BAS11	56	1259	Coarse Silt	8.39	76.13	9.08	5.81	9.68	Qtz, Di, Pl, Or, Ol, Hem, Ms, Cal, Om	Quartzites, granites	WS	Medium	Sub-rounded	Low sphericity	P
BAS12	355	1042	Medium Sand	16.79	69.47	4.14	3.56	10.18	Qtz, Pl, Cal, Di, Ms, Bt, Hem, Om	Quartzites, phyllites, granites, bioclasts (traces)	MWS	Medium	Sub-angular	High sphericity	P
BAS13	274	4336	Medium Sand	14.51	73.28	5.05	4.23	7.98	Qtz, Pl, Di, Or, Cal, Hem, Om	Quartzites, granites, trachy-andesites (traces)	MWS	Medium	Sub-angular	High sphericity	P
BAS14	328	1141	Medium Sand	8.64	79.47	9.20	7.26	4.63	Qtz, Pl, Cal, Di, Or, Ms, Bt, Hem, Om	Quartzites, granites, trachy-basalts (traces)	PS	Low	Sub-angular	Low sphericity	P
BAS15	223	2222	Fine Sand	11.07	75.49	6.82	5.14	8.30	Qtz, Pl, Cal, Hem, Or, Om	Quartzites, rhyolites (traces)	WS	Medium	Sub-rounded	High sphericity	P
BAS16	362	1296	Medium Sand	8.10	76.32	9.42	9.35	6.23	Qtz, Cal, Pl, Di, Or, Hem, Bt, Om	Quartzites, granites, rhyolites (traces), basaltic trachy-andesites (traces), trachytes (traces)	MS	Low	Sub-angular	High sphericity	P
BAS17	200	1362	Fine Sand	12.29	82.01	6.67	4.20	1.50	Qtz, Pl, Cal, Di, Or, Hem, Ms, Bt, Om	Quartzites, granites, phyllites	WS	High	Sub-rounded	High sphericity	P
BAS18	210	879	Fine Sand	7.21	85.89	11.91	5.96	0.94	Qtz, Cal, Pl, Hem, Ms, Bt, Om	Quartzites, phyllites, granites, andesites (traces)	WS	Low	Sub-angular	High sphericity	P
BAS19	270	1277	Medium Sand	27.35	62.82	2.30	7.48	2.35	Qtz, Pl, Cal, Hem, Di, Ms, Bt, Om	Quartzites, granites, phyllites	PS	High	Sub-rounded	Low sphericity	P
BAS20	260	1864	Medium Sand	14.72	77.59	5.27	6.76	0.93	Qtz, Pl, Or, Ms, Di, Cal, Om	Quartzites, granites, phyllites	VWS	Medium	Sub-angular	High sphericity	P
BAS21	123	2271	Very Fine Sand	5.09	89.06	17.48	4.91	0.94	Qtz, Pl, Or, Di, Hem, Bt, Ms, Cal, Om	Quartzites, phyllites, trachy-andesites (traces), dacites (traces)	MWS	Medium	Angular	High sphericity	P
BAS22	387	1715	Medium Sand	6.34	87.97	13.87	3.90	1.79	Qtz, Or, Pl, Di, Hem, Ms, Om, Cal	Quartzites, granites, trachy-basalts (traces)	PS	Medium	Sub-angular	Low sphericity	P
BAS23	123	901	Very Fine Sand	10.20	81.63	8.00	0.00	8.16	Qtz, Pl, Di, Or, Hem, Cal, Om	Quartzites, phyllites	MWS	Medium	Sub-rounded	Low sphericity	A
BAS24	464	1141	Medium Sand	6.46	86.69	13.42	4.11	2.74	Qtz, Pl, Di, Or, Cal, Hem, Ms, Bt, Om	Quartzites, phyllites, trachy-andesites (traces), trachytes (traces)	WS	Low	Sub-rounded	High sphericity	P
BAS25	86	1955	Very Fine Sand	15.81	74.42	4.71	6.28	3.49	Qtz, Cal, Pl, Or, Di, Hem, Ms, Om	Quartzites, granites	WS	Low	Sub-rounded	Low sphericity	P
BAS26	290	2225	Medium Sand	15.27	74.25	4.86	8.68	1.80	Qtz, Pl, Or, Di, Hem, Cal, Om	Quartzites, granites, phyllites, sandstones (traces), trachytes (traces), dacites (traces)	MWS	High	Sub-rounded	Low sphericity	P
BAS27	260	694	Medium Sand	6.10	91.08	14.92	1.88	0.94	Qtz, Di, Pl, Or, Cal, Hem, Om	Quartzites, granites	MWS	Low	Sub-rounded	High sphericity	P
BAS28	92	557	Very Fine Sand	10.87	78.26	7.20	8.70	2.17	Qtz, Pl, Chl, Gp, Hem, Om, Cal	Quartzites, granites	PS	High	Sub-rounded	High sphericity	A
BAS29	60	423	Coarse Silt	9.09	75.76	8.33	13.64	1.52	Qtz, Pl, Cal, Or, Ms, Di, Hem, Om	Quartzites, granites	WS	Low	Sub-rounded	High sphericity	A

Table 2. Petrographic features of the brick samples on thin section [Sorting: MS: moderately sorted, MWS: moderately well sorted, PS: poorly sorted, VWS: very well sorted, WS: well sorted. Mineralogical phases: Bt: biotite, Cal: calcite, Chl: chlorite, Di: diopside, Gy: gypsum, Hem: hematite, Ms: muscovite, Ol: olivine, Om: opaque minerals, Or: orthoclase, Pl: plagioclase, Qtz: quartz. Chamotte: A: absent, P: present].

	Matrix	Monomineralic fragments	Polimineralic fragments	Porosity d> 1/16 mm	Chamotte	Secondary calcite inside pores	Sum
BAS1	88.75	2.70	0.56	2.25	0.34	5.40	100
BAS2	78.47	3.47	3.82	6.08	n.d.	8.16	100
BAS3	75.03	9.30	7.90	5.73	1.02	1.02	100
BAS4	66.93	4.08	6.90	4.39	11.60	6.11	100
BAS5	85.06	1.30	4.55	3.25	n.d.	5.84	100
BAS6	86.08	1.87	1.19	4.24	n.d.	6.62	100
BAS7	75.42	3.23	9.13	4.63	0.56	7.02	100
BAS8	84.36	2.50	3.99	4.66	0.83	3.66	100
BAS9	71.99	3.95	7.22	7.39	n.d.	9.45	100
BAS10	83.66	2.14	6.42	4.28	n.d.	3.50	100
BAS11	76.13	3.44	4.52	5.81	0.43	9.68	100
BAS12	69.47	3.05	13.23	3.56	0.51	10.18	100
BAS13	73.28	2.66	11.37	4.23	0.48	7.98	100
BAS14	79.47	1.63	6.01	7.26	1.00	4.63	100
BAS15	75.49	2.77	7.91	5.14	0.40	8.30	100
BAS16	76.32	2.49	5.30	9.35	0.31	6.23	100
BAS17	82.01	4.05	8.10	4.20	0.15	1.50	100
BAS18	85.89	0.31	5.96	5.96	0.94	0.94	100
BAS19	62.82	1.50	25.21	7.48	0.64	2.35	100
BAS20	77.59	2.25	12.07	6.76	0.40	0.93	100
BAS21	89.06	2.08	1.70	4.91	1.32	0.94	100
BAS22	87.97	1.46	4.55	3.90	0.33	1.79	100
BAS23	81.63	4.08	6.12	0.01	n.d.	8.16	100
BAS24	86.69	0.98	5.28	4.11	0.20	2.74	100
BAS25	74.42	3.72	6.98	6.28	5.12	3.49	100
BAS26	74.25	1.20	13.17	8.68	0.90	1.80	100
BAS27	91.08	1.88	3.76	1.88	0.47	0.94	100
BAS28	78.26	2.17	8.70	8.70	n.d.	2.17	100
BAS29	75.76	3.03	6.06	13.64	n.d.	1.52	100

Table 3 Results of the modal analysis of the bricks (% by vol.), performed by a point-counter placed on the table of the polarized microscope; n.d. = not detected.

	Max. <----------> Min.						
BAS1	Qtz	Pl	Di	Cal	Hem		
BAS2	Qtz	Pl	Di	Hem	Cal		
BAS3	Qtz	Pl	Hem				
BAS4	Qtz	Pl	Or	Di	Cal	Mca	Hem
BAS5	Qtz	Cal	Di	Pl	Or	Hem	
BAS6	Qtz	Di	Pl	Or	Hem		
BAS7	Qtz	Di	Pl	Cal	Or		
BAS8	Qtz	Pl	Or	Di	Cal	Mca	Hem
BAS9	Qtz	Pl	Di	Or	Cal	Hem	
BAS10	Qtz	Di	Pl	Mca	Hem		
BAS11	Qtz	Di	Pl	Or	Ol	Hem	
BAS12	Qtz	Pl	Cal	Di	Mca	Hem	
BAS13	Qtz	Pl	Di	Or	Cal	Hem	
BAS14	Qtz	Pl	Cal	Di	Or	Mca	Hem
BAS15	Qtz	Pl	Cal	Hem	Or		
BAS16	Qtz	Cal	Pl	Di	Or	Hem	
BAS17	Qtz	Pl	Cal	Di	Or	Hem	
BAS18	Qtz	Cal	Pl	Hem	Mca		
BAS19	Qtz	Pl	Cal	Hem	Di		
BAS20	Qtz	Pl	Or	Mca	Di		
BAS21	Qtz	Pl	Or	Di	Hem		
BAS22	Qtz	Or	Pl	Di	Hem		
BAS23	Qtz	Pl	Di	Or	Hem		
BAS24	Qtz	Pl	Di	Or	Cal	Hem	
BAS25	Qtz	Cal	Pl	Or	Di	Hem	
BAS26	Qtz	Pl	Or	Di	Hem		
BAS27	Qtz	Di	Pl	Or	Cal	Hem	
BAS28	Qtz	Pl	Chl	Gp	Hem		
BAS29	Qtz	Pl	Cal	Or	Mca	Di	Hem

Table 4 Qualitative mineralogical composition of the samples in order of decreasing relative abundance, detected by XRPD analysis (Cal: calcite; Chl: chlorite; Di: diopside; Gp: gypsum; Hem: hematite; Mca: micas; Ol: olivine; Or: orthoclase; Pl: plagioclase; Qtz: quartz).

% wt	SiO_2	TiO_2	Al_2O_3	Fe_2O_3	MnO	MgO	CaO	Na_2O	K_2O	P_2O_5	LOI	Sum
BAS1	49.63	0.86	16.94	10.02	0.18	5.98	10.41	1.53	2.20	0.09	2.16	100
BAS2	50.02	0.90	15.10	10.38	0.16	8.50	10.03	1.31	1.77	0.09	1.74	100
BAS3	64.17	1.44	17.36	8.63	0.17	2.44	1.37	1.65	1.64	0.08	1.05	100
BAS4	53.85	0.93	14.94	9.54	0.17	4.65	9.77	1.22	2.47	0.11	2.35	100
BAS5	49.56	0.74	12.89	8.79	0.16	4.25	15.05	1.34	1.62	0.11	5.49	100
BAS6	48.83	0.81	14.28	9.37	0.14	9.17	10.88	1.52	1.65	0.10	3.25	100
BAS7	51.37	0.66	12.37	8.39	0.16	4.93	15.90	1.45	1.13	0.07	3.57	100
BAS8	51.01	0.79	17.16	8.72	0.14	6.30	10.02	1.48	2.24	0.10	2.04	100
BAS9	54.25	0.83	13.49	8.91	0.14	7.60	9.82	1.25	1.49	0.10	2.12	100
BAS10	48.41	0.81	13.82	9.25	0.14	8.83	11.50	1.70	1.91	0.10	3.53	100
BAS11	54.23	0.91	15.10	9.36	0.16	7.74	8.25	1.08	1.72	0.09	1.36	100
BAS12	52.54	0.86	13.58	9.21	0.15	7.45	10.55	1.09	1.60	0.09	2.88	100
BAS13	54.01	0.82	13.75	8.84	0.14	7.47	10.08	1.13	1.51	0.10	2.15	100
BAS14	49.38	0.73	16.15	8.23	0.13	5.56	11.21	1.69	2.12	0.09	4.71	100
BAS15	51.10	0.81	14.41	8.89	0.16	6.08	10.78	1.64	1.60	0.11	4.42	100
BAS16	38.98	0.88	11.69	12.63	0.18	3.70	19.02	1.15	2.26	0.10	9.41	100
BAS17	55.40	0.86	19.96	7.51	0.14	2.99	4.83	1.18	3.27	0.08	3.78	100
BAS18	48.66	0.89	16.63	9.24	0.16	5.55	8.07	0.81	2.32	0.13	7.54	100
BAS19	62.00	1.05	15.43	7.70	0.13	3.15	5.41	1.49	1.93	0.14	1.57	100
BAS20	60.68	1.14	19.45	7.13	0.10	3.22	1.49	1.78	2.45	0.11	2.45	100
BAS21	51.75	1.06	18.36	9.99	0.16	6.45	5.14	0.80	2.53	0.13	3.63	100
BAS22	51.88	0.99	15.53	9.56	0.10	4.34	5.70	0.86	2.91	2.78	5.35	100
BAS24	50.68	0.80	16.24	9.04	0.15	5.66	10.73	1.44	2.07	0.09	3.10	100
BAS26	57.72	0.79	12.52	8.03	0.13	7.12	8.88	1.44	1.35	0.11	1.91	100
BAS27	49.62	0.81	13.70	9.54	0.15	8.65	12.48	1.13	1.57	0.10	2.25	100

Table 5 Content of the major chemical elements of the bricks of Hagia Sophia, performed on the bulk samples by XRF analysis.

ppm	Ni	Cr	V	La	Ce	Co	Ba	Nb	Y	Sr	Zr	Rb
BAS1	276	345	136	19	24	39	287	15	29	314	83	105
BAS2	465	528	129	19	38	48	354	13	29	209	71	93
BAS3	86	171	119	22	97	29	419	13	30	73	202	69
BAS4	204	317	124	23	67	31	424	23	32	200	129	120
BAS5	122	274	132	22	47	29	403	33	29	231	98	87
BAS6	366	502	119	30	29	43	401	19	27	225	61	89
BAS7	151	259	119	19	42	29	344	22	30	276	53	77
BAS8	248	306	150	21	40	38	318	13	29	342	60	102
BAS9	330	483	130	19	37	37	271	12	27	240	65	79
BAS10	314	474	151	19	37	37	270	16	27	220	69	90
BAS11	402	521	143	19	36	39	313	12	31	139	70	88
BAS12	321	550	139	19	37	40	339	14	27	200	71	79
BAS13	349	522	137	19	36	34	242	12	28	191	58	81
BAS14	166	287	150	27	38	34	326	19	26	408	74	98
BAS15	211	407	127	19	44	37	365	18	28	359	93	82
BAS16	102	300	109	19	44	19	154	27	21	367	148	91
BAS17	106	212	115	38	51	27	600	37	37	133	142	150
BAS18	194	463	135	19	36	38	364	27	26	183	126	106
BAS19	119	209	122	28	67	25	406	16	31	110	146	90
BAS20	91	219	120	26	43	25	451	23	35	117	173	105
BAS21	299	447	152	19	50	45	361	23	24	154	123	120
BAS22	215	360	105	19	44	29	394	19	19	304	183	120
BAS24	211	286	177	21	51	33	299	13	26	358	71	98
BAS26	303	526	128	19	34	36	294	10	26	181	62	72
BAS27	401	509	139	27	24	44	330	15	29	202	48	84

Table 6 Content of the trace chemical elements of the bricks of Hagia Sophia, performed on the bulk samples by XRF analysis.

% wt	Weight loss T<120 °C	Weight loss 120<T<200 °C	Weight loss 200<T<400 °C	Weight loss 400<T<600 °C	Weight loss 600<T<650 °C	Weight loss T>650 °C	Weight loss Total 30<T<920 °C	CO_2	SBW	CO_2/SBW
BAS1	0.36	0.24	0.44	0.40	0.29	0.76	2.49	1.26	0.87	1.45
BAS2	0.18	0.14	0.28	0.24	0.17	0.63	1.64	0.85	0.61	1.39
BAS3	0.08	0.12	0.41	0.15	0.14	0.10	1.00	0.25	0.67	0.37
BAS4	0.18	0.12	0.31	0.20	0.16	0.78	1.75	0.97	0.60	1.62
BAS5	0.49	0.31	0.61	0.54	0.33	3.19	5.47	3.68	1.30	2.83
BAS6	0.37	0.31	0.53	0.79	0.36	0.37	2.73	0.81	1.55	0.52
BAS7	0.34	0.19	0.39	0.28	0.21	2.10	3.51	2.37	0.80	2.96
BAS8	0.26	0.14	0.29	0.27	0.30	0.78	2.04	1.06	0.72	1.47
BAS9	0.24	0.14	0.30	0.27	0.19	1.19	2.33	1.34	0.75	1.79
BAS10	0.53	0.28	0.77	0.91	0.25	0.94	3.68	0.48	2.67	0.18
BAS11	0.11	0.10	0.34	0.23	0.20	0.29	1.27	0.49	0.67	0.73
BAS12	0.26	0.14	0.33	0.36	0.25	1.20	2.54	1.44	0.84	1.71
BAS13	0.29	0.19	0.49	0.28	0.17	0.67	2.09	0.90	0.90	1.00
BAS14	0.41	0.22	0.44	0.68	0.38	2.27	4.40	2.71	1.28	2.12
BAS15	0.27	0.17	0.45	0.37	0.20	2.67	4.13	2.80	1.06	2.64
BAS16	1.30	0.51	1.34	2.20	0.95	3.69	9.99	3.79	4.90	0.77
BAS17	0.47	0.39	0.80	0.40	0.24	1.49	3.79	1.66	1.66	1.00
BAS18	1.29	0.80	0.97	0.81	0.36	3.16	7.39	3.50	2.60	1.35
BAS19	0.31	0.21	0.55	0.31	0.17	1.39	2.94	1.60	1.03	1.55
BAS20	1.05	0.32	0.44	0.53	0.32	0.43	3.09	0.72	1.32	0.55
BAS21	2.42	0.80	1.25	0.76	0.05	0.19	5.47	0.77	2.28	0.34
BAS22	2.85	1.88	1.50	0.53	0.11	0.20	7.07	0.29	3.93	0.07
BAS23	0.14	0.13	0.42	0.27	0.17	1.15	2.28	1.37	0.77	1.78
BAS24	0.30	0.23	0.44	0.63	0.26	0.65	2.51	1.38	0.83	1.66
BAS25	0.71	0.38	0.78	0.67	0.38	3.35	6.27	4.00	1.56	2.56
BAS26	0.21	0.11	0.26	0.24	0.19	0.58	1.59	0.81	0.57	1.42
BAS27	0.18	0.16	0.27	0.21	0.18	0.72	1.72	0.95	0.59	1.61
BAS28	0.14	0.43	0.59	0.18	0.18	0.19	1.71	0.37	1.20	0.31
BAS29	0.34	0.46	1.60	1.15	0.43	2.16	6.14	3.05	2.75	1.11

Table 7 Results of the TGA analysis of the bricks of Hagia Sophia; SBW=structurally bound water.

% wt	SiO_2	TiO_2	Al_2O_3	Fe_2O_3	MnO	MgO	CaO	Na_2O	K_2O	P_2O_5	Sum
BAS1	53.41	0.78	19.90	7.37	0.20	4.60	8.59	1.91	2.92	0.27	100
BAS2	54.57	0.79	16.94	8.20	0.18	6.80	8.19	1.47	2.26	0.26	100
BAS3	71.32	1.15	15.19	5.13	0.12	1.45	0.53	3.10	1.70	0.32	100
BAS4	59.53	0.73	15.58	6.53	0.09	3.46	9.30	2.02	2.48	0.28	100
BAS5	54.64	0.82	18.35	7.39	0.28	5.19	8.38	2.38	2.29	0.26	100
BAS6	54.73	0.91	17.58	8.28	0.30	6.91	6.67	1.79	2.61	0.21	100
BAS7	54.33	0.77	15.13	6.88	0.15	4.06	15.55	1.51	1.43	0.21	100
BAS8	54.66	0.84	18.00	7.17	0.21	4.74	9.61	1.77	2.85	0.16	100
BAS9	56.48	0.80	16.37	7.87	0.16	5.97	8.64	1.48	2.01	0.23	100
BAS10	51.72	0.84	15.71	7.65	0.21	6.96	12.58	1.81	2.28	0.25	100
BAS11	57.03	0.92	17.07	8.37	0.26	6.45	5.79	1.38	2.50	0.24	100
BAS12	57.30	1.04	15.40	7.45	0.25	5.92	8.91	1.59	1.95	0.17	100
BAS13	58.87	0.73	15.13	7.04	0.15	5.79	8.52	1.45	2.04	0.26	100
BAS14	54.37	0.85	19.36	7.03	0.21	4.72	8.60	1.75	2.86	0.25	100
BAS15	55.93	0.82	17.84	7.51	0.14	5.45	7.68	1.98	2.42	0.23	100
BAS16	53.84	0.81	18.17	6.94	0.19	4.46	10.53	2.05	2.70	0.30	100
BAS17	60.56	0.76	22.21	6.42	0.20	1.56	2.03	1.53	4.44	0.27	100
BAS18	55.82	0.78	17.22	7.41	0.21	4.08	9.89	1.25	3.05	0.28	100
BAS19	68.88	0.82	15.63	5.65	0.13	1.92	1.80	2.73	2.14	0.31	100
BAS20	63.23	1.19	19.07	7.39	0.16	2.25	0.51	2.53	3.41	0.26	100
BAS21	56.74	0.87	19.16	7.47	0.24	4.55	5.91	1.68	3.02	0.35	100
BAS22	53.42	0.85	18.07	7.79	0.16	3.79	6.81	0.97	3.05	5.08	100
BAS23	54.15	0.82	15.40	7.78	0.22	7.18	10.39	1.65	2.16	0.26	100
BAS24	54.38	0.76	19.07	7.29	0.21	4.59	9.23	1.54	2.71	0.23	100
BAS25	55.04	0.76	16.66	5.87	0.37	3.89	12.90	1.52	2.68	0.31	100
BAS26	56.19	0.76	15.99	7.33	0.20	6.16	9.20	1.67	2.12	0.38	100
BAS27	52.98	0.86	15.55	7.77	0.19	6.75	12.15	1.50	2.05	0.20	100
BAS28	66.21	0.93	17.61	6.44	0.19	2.26	0.89	2.69	2.31	0.47	100
BAS29	66.01	1.11	17.30	6.66	0.17	2.14	1.02	2.49	2.56	0.53	100

Table 8 Content of the major chemical elements of the matrix for the bricks of Hagia Sophia, performed by micro-EDS analysis obtained as mean value calculated on three representative areas of the matrix 600X600 μm^2 in size.